Mean-Shift Distillation for Diffusion Mode Seeking

Vikas Thamizharasan [1 2] **Nikitas Chatzis** [3] **Iliyan Georgiev** [2] **Matthew Fisher** [2] **Evangelos Kalogerakis** [1 4]
Difan Liu [2] **Nanxuan Zhao** [2] **Michal Lukáč** [2]

Abstract

We present *mean-shift distillation*, a novel diffusion distillation technique that provides a provably good proxy for the gradient of the diffusion output distribution. This is derived directly from mean-shift mode seeking on the distribution, and we show that its extrema are aligned with the modes. We further derive an efficient product distribution sampling procedure to evaluate the gradient.

Our method is formulated as a drop-in replacement for score distillation sampling (SDS), requiring neither model retraining nor extensive modification of the sampling procedure. We show that it exhibits superior mode alignment as well as improved convergence in both synthetic and practical setups, yielding higher-fidelity results when applied to both text-to-image and text-to-3D applications with Stable Diffusion.

This work is based on the Arxiv preprint *Mean-Shift Distillation for Diffusion Mode Seeking* (Thamizharasan et al., 2025). See https://www.arxiv.org/abs/2502.15989.

Keywords: Other, Vision and Learning

1. Introduction

Soon after image diffusion (Dhariwal & Nichol, 2021) models exploded in popularity, DreamFusion (Poole et al., 2022) and SJC (Wang et al., 2022) concurrently introduced the idea of using them for image optimization. Intuitively, this can be expressed as the notion that images more likely to be generated by a diffusion model are "better" in the sense of being more faithful to the data distribution the diffusion model was trained on.

Formally, diffusion models provide a mechanism to sample images $x \in \mathcal{I}$ from a learned distribution $p(x)$. We then have a parameter vector $\vartheta \in \mathcal{P}$, along with an image-generating model $g : \mathcal{P} \to \mathcal{I}$. Given an initialization ϑ^0, we seek to optimize a ϑ^k such that $p(g(\vartheta^k)) > p(g(\vartheta^0))$. We expect this to yield an image $g(\vartheta^k)$ of higher quality, under the metric the diffusion model is trained for.

We could imagine optimizing ϑ by determining the gradient $\nabla p(g(\vartheta))$ and ascending along it. However, while we may use our diffusion model to sample from $p(x)$, we can neither easily evaluate $p(x)$ nor determine its gradient $\nabla_x p(x)$. Even though we can formally express $p(x)$ in terms of the score function $\epsilon(x, t)$ through the instantaneous change of variable formula (Grathwohl et al., 2019), evaluating this formula requires calculating the divergence of the score function along the entire ODE path, making this of only theoretical interest. Evaluating the gradient of this quantity is even less practical.

Score distillation sampling (SDS) (Poole et al., 2022; Wang et al., 2022) attempts to address this problem by offering proxies for the density gradient that are easier to estimate. However, their theoretical properties are not rigorously established, and SDS suffers from significant bias as well as variance, yielding inaccurate gradients. Examining the loss landscape of SDS in Figure 1, we indeed see that not only are the maxima of this function not collocated with the modes of $p(x)$, but even in the simplest cases the loss creates "phantom modes" that are well out of distribution. Our method offers both better alignment with the distribution and lower variance of the gradient estimate.

Contributions. In this paper, we propose *mean-shift distillation*, a distribution-gradient proxy based on a well-known mode-seeking technique. Furthermore, we show that:

- This proxy can be implemented easily, with minimal changes to the diffusion sampling procedure;
- It evaluates with less variance than SDS with improved mode alignment;
- It has superior behavior, converging to modes of the trained distribution with a clear termination criterion.

[1]University of Massachusetts, Amherst [2]Adobe Research [3]National Technical University of Athens [4]TU Crete . Correspondence to: Vikas Thamizharasan <vthamizharas@umass.edu>.

2. Related Work

Denoising diffusion. In our work we rely most directly on the mean-shift method of mode seeking (Cheng, 1995; Comaniciu & Meer, 2002), but our ability to apply it to diffusion rests on a body of theoretical analysis of this process.

Mathematically, denoising diffusion consists of solving an initial value problem (IVP) on a random variable from a simple, typically standard normal distribution, where the time-dependent gradient is learned by reversing the process of adding noise to the distribution being modeled (Song et al., 2021b;a). Already in these works authors suggest ways in which the output distribution may be manipulated by adding terms to the differential equation underlying the initial value problem, a property we will rely on to manipulate the output to our method's advantage.

A surprising connection between mean shift and diffusion emerged from the analysis of the optimal denoising model (Karras et al., 2022; Chen et al., 2024; Je et al., 2024). Since the forward (noising) process can be expressed as successive convolutions with a Gaussian kernel, the intermediate distributions are in fact Gaussian-kernel density estimates of the data distributions, with kernel bandwidth proportional to the time parameter. Therefore in the ODE of the reverse (inference) process, the gradient of the denoiser is theoretically equal to the mean-shift vector with appropriate kernel and bandwidth. Mean-shifting on the IVP time domain does not in fact seek modes of the output distribution, but we take advantage of this knowledge to implement mean shift on that domain.

Further related to the analysis of modes in particular, (Karras et al., 2024; Bradley & Nakkiran, 2024) suggest that applying classifier-free guidance (CFG) (Ho & Salimans, 2021) to diffusion has the effect of sharpening the modes of the output distribution. This guidance does not explicitly *seek* modes, but we have found that using CFG synergizes well with both SDS and our method.

Distilling diffusion priors. Score distillation sampling (SDS) (Poole et al., 2022; Wang et al., 2022) has emerged as a useful technique for leveraging the priors learned by large-scale image models beyond 2D raster images. SDS provides an optimization procedure to estimate the parameters of a differentiable image generator, such that the rendered image is pushed towards a higher-probability region of a pre-trained prompt-conditioned image diffusion model. Originally proposed to optimize volumetric representations like NeRFs, it has been extended to other non-pixel-based representations (Jain et al., 2023; Yi et al., 2024; Bahmani et al., 2024; Thamizharasan et al., 2024).

The tendency of SDS to produce over-smoothened results due to high variance is well documented. A plethora of works have been proposed to mitigate this behavior, e.g. to factorize the gradient to reduce the bias (Hertz et al., 2023; Yu et al., 2024; Katzir et al., 2024; Alldieck et al., 2024), or to replace the uniform noise sampling in SDS with noise obtained by running DDIM inversion (Liang et al., 2023; Lukoianov et al., 2024). SteinDreamer (Wang et al., 2023a) propose a control variate for SDS, (Xu et al., 2024; Yan et al., 2025) improve diversity of generations, and (Wang et al., 2024) alleviate the multi-view inconsistency problem.

VSD (Wang et al., 2023b) tackle the low-fidelity problem by treating the target parameters as a random variable and estimate the variational distribution to produce diverse, high-fidelity results. SDI (Lukoianov et al., 2024), on the other hand and unlike previous variance-reduction methods, find a better approximation of the added noise term, eliminating one of the root causes of the excessive variance. These methods attribute SDS/SJC to be mode-seeking; we show it is not and introduce mode-seeking behavior to address the excessive variance and low-fidelity results.

We draw the distinction between the above methods to knowledge distillation works designed for one-step inference (Yin et al., 2024; Luo et al., 2023; Xie et al., 2024). Diff-Instruct (Luo et al., 2023) show that SDS is a special case of their distillation formulation when the generator's output is a Dirac's Delta distribution and the marginal of the variational score is Gaussian. While the derived gradients resemble SDS and VSD, these methods require training an auxiliary score network to estimate the variational score— challenging to generalize beyond text-to-image generation— and have been targeted for different use cases, namely faster inference, model compression, and dataset privacy-preserving.

3. Mean-Shift Distillation

In this section we derive the mean-shift vector for the diffusion output distribution, and show how it approximates the gradient thereof. We further show how an efficient estimate of this vector may be obtained with a minimal modification of diffusion sampling. We begin with a motivation of our development by illustrating the pitfalls of SDS.

3.1. Motivation

Given a pre-trained diffusion model ϵ_ϕ, the SDS loss penalizes the KL-divergence of a unimodal Gaussian distribution centered around x and the data distribution $p_\phi(z_t; c, t)$ captured by the frozen diffusion model conditioned on text embeddings c. With $x = g(\vartheta)$, an image rendered by ϑ via a differentiable renderer g, (Poole et al., 2022) derive the

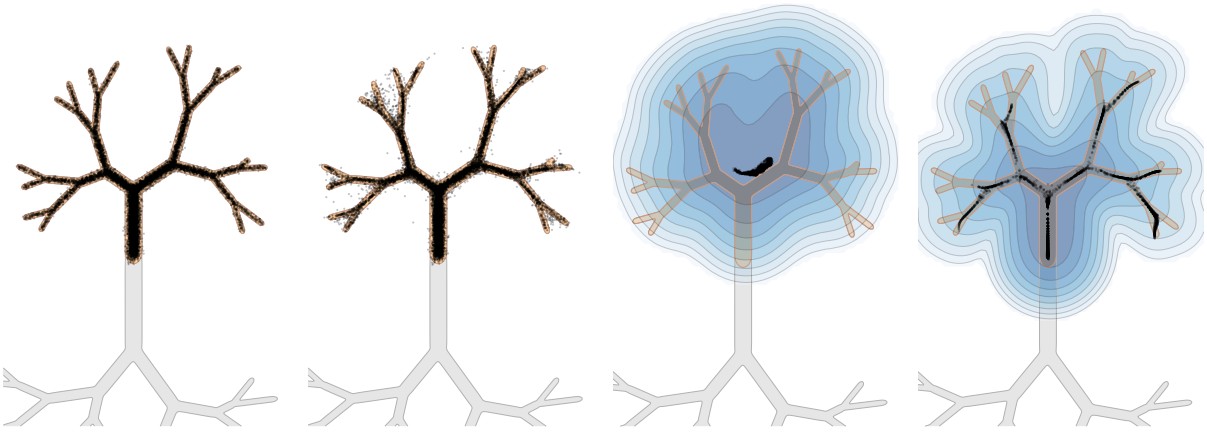

(a) Ground truth (b) DDIM (c) SDS (d) **Our MSD**

• data sample loss landscape

Figure 1: Mode-seeking simulated in a fractal-like 2D distribution with two (orange, gray) classes, adapted from (Karras et al., 2024). We compare the behavior of diffusion sampling (DDIM) to optimization-based diffusion distillation, in a class-conditional setting. With class=orange, **(a)** Ground truth distribution, **(b)** DDIM sampling , **(c)** SDS, and **(d)** our MSD. All methods are run without guidance.

gradient of the loss $\mathcal{L}_{\text{SDS}}$ with respect to ϑ:

$$\nabla_\vartheta \mathcal{L}_{\text{SDS}} = \mathbb{E}_{t,\epsilon}\Big[\alpha(t)\left(\epsilon_\phi(\alpha(t)x + \epsilon; t) - \epsilon\right)\Big]\frac{\partial x}{\partial \vartheta},$$
$$\text{with } t \sim U(0,T), \epsilon \sim \mathcal{N}(0, \sigma(t)I). \quad (1)$$

To illustrate the pitfalls of SDS, we simulate it in 2D using a small denoising diffusion network (Figure 1). This allows us to set $\vartheta = x \in \mathbb{R}^2$ (where g becomes an identity map). We construct a fractal-like dataset as shown by (Karras et al., 2024), with analytic ground-truth probability density and score. This data distribution is a mixture of highly anisotropic Gaussians, where most of the probability mass resides in narrow regions, emulating the low intrinsic dimensionality of natural images (Roweis & Saul, 2000; Belkin & Niyogi, 2003). For a baseline, we compare it with DDIM (Song et al., 2021a), a popular first-order sampling algorithm, with classifier-free guidance (CFG) (Ho & Salimans, 2021). More details can be found in Section 4.2.

It is immediately apparent how even in this simple setting, the optima to which SDS converges do not model the output distribution well. Furthermore, the convergence itself is problematic due to very high variance of SDS, which we will address later.

3.2. Mean-shift Gradient Approximation

We start by convolving the data density p with a radial Gaussian kernel $G_\lambda(x) = c_\lambda e^{-x^2/\lambda^2}$ with bandwidth λ, normalized by a constant c_λ. This convolution yields a smoothed density $p^*_\lambda(x)$:

$$p^*_\lambda(x) = p * G_\lambda(x) = \int G_\lambda(x-y)p(y)dy. \quad (2)$$

We now take the gradient $\nabla_x p^*_\lambda(x)$ of the smoothed density and substitute the Gaussian kernel's gradient:

$$\nabla_x p^*_\lambda(x) = \int \nabla_x G_\lambda(x-y)p(y)dy \quad (3)$$
$$= \int c_\lambda(x-y)G_\lambda(x-y)p(y)dy. \quad (4)$$

We then take the stationary-point equation and reorganize it as a fixed-point iteration:

$$\nabla_x p^*_\lambda(x) = 0 \implies x' = \frac{\int yG_\lambda(x-y)p(y)dy}{\int G_\lambda(x-y)p(y)dy}, \quad (5)$$

where the constant c_λ cancels out. We will discuss the practical estimation of the integrals in Section 3.3 below.

The iterative process in Equation (5) is a continuous version of mean shift (Comaniciu & Meer, 2002). We may turn this into gradient proxy with several desirable properties. Defining the mean-shift vector $\vec{m}(x) = x' - x$, it follows from Equation (3) that

$$\vec{m}(x) \propto p^*_\lambda(x)\nabla_x p^*_\lambda(x). \quad (6)$$

Since the smoothed density $p^*_\lambda(x)$ is always non-negative, $\vec{m}(x)$ is always aligned with its gradient $\nabla p^*_\lambda(x)$. It is also aligned with the gradient of the true density p as $\lambda \to 0$ (when such gradient exists). This means that a differential step along the vector $\vec{m}(x)$ will improve the likelihood of x, making this a good proxy for the kernel density estimation gradient. Furthermore, it implies that $\vec{m}(x)$ will be zero at the modes of $p^*_\lambda(x)$, giving us a convergence criterion.

3.3. Gradient Estimation via Product Sampling

The integrals in Equation (5) can be both estimated using samples y from the density p; such estimation yields the classical mean-shift expression

$$x' = \frac{\sum_{y_i \sim p} G_\lambda(x - y_i) y_i}{\sum_{y_i \sim p} G_\lambda(x - y_i)}. \tag{7}$$

In our case, we do not have such samples readily available. We could in theory use images from the training dataset as these samples, or else use the diffusion model to generate them – either as a pre-process or on-the-fly during iteration. Unfortunately, that would be prohibitively costly as the datasets are typically quite large and accurate estimation would require a very large number of samples for practical (i.e. small) kernel bandwidths λ.

Our key insight is that the right-hand side of Equation (5) can be viewed as an expectation with respect to a density $\dot{p}_\lambda$ that is the product of p and the kernel G_λ centered at x:

$$x' = \int y \, \dot{p}_\lambda(y|x) dy \; = \; \mathbb{E}_{y \sim \dot{p}_\lambda(y|x)}[y]. \tag{8}$$

To generate samples y from this product density, we exploit the fact that diffusion models employ score-based sampling (Song et al., 2021b; Dhariwal & Nichol, 2021). Instead of using the score $\nabla \log p$ of the density p in DDIM sampling, we use the score of our product density:

$$\begin{aligned} \nabla_{z_t} \log(\dot{p}_\lambda(y|x)) &= \nabla_{z_t} \log p(z_t) + \nabla_{z_t} \log G_\lambda(x - z_t) \\ &= \nabla_{z_t} \log p(z_t) - \frac{x - z_t}{\lambda^2}, \end{aligned} \tag{9}$$

where $z_t = \alpha(t)x + \epsilon$. This is the sum of the density score (provided by the diffusion model) and the score of our Gaussian kernel. Having the ability to generate samples y_i from the product density, we can estimate the mean-shift iterate (8) as

$$x' \approx \frac{1}{N} \sum_{y_i \sim \dot{p}_\lambda(y|x)} y_i. \tag{10}$$

In practice we use a single sample y, which simplifies our mean-shift vector to

$$\vec{m}(x) = y - x. \tag{11}$$

We can thus step along $\vec{m}$ to seek the modes of the data density p. Substituting a learned score model into 9 gives us

$$\hat{\epsilon}_t = \epsilon_\theta(z_t; t) - \frac{x - z_t}{\lambda^2}. \tag{12}$$

3.4. Practical Considerations

As noted in SJC (Wang et al., 2022), distillation with unconditioned diffusion models is challenging in high-dimensional settings like images. While we show unconditioned diffusion distillation is practical in simple 2D toy datasets below, we operate in the conditional setting throughout.

Impact of guidance. Conditional score estimates from diffusion models, $\epsilon_\theta(z_t, c) \approx -\sigma_t \nabla_{z_t} \log p(z_t|c)$, are improved in practice with classifier-free guidance (CFG) (Ho & Salimans, 2021), which sharpens the distribution around the modes:

$$\tilde{\epsilon}_\theta(z_t, c) = (1 + w)\epsilon_\theta(z_t, c) - w\epsilon_\theta(z_t). \tag{13}$$

We may directly substitute this for the denoiser term in Equation (12). Despite its practical success, the denoising direction induced by CFG does not provide theoretical guarantees in producing samples from $p_{0,w}(z_t|c)$ (Bradley & Nakkiran, 2024). Even in simple settings, as observed in Figure 1(b), CFG can lead to mode drops. While alternative guidance strategy exists (Karras et al., 2024), we stick with the dominant practice of using CFG (Equation (13)). We have found that this synergizes well with mode-seeking by mean-shift, and show the effects of this in evaluation below. See discussion in Appendix B.

Integrating kernel score. Because the magnitude of the kernel term in Equation (12) can be quite high when $|y - z_t|$ is high relative to λ, directly implementing this can result in instability while denoising particularly with explicit integrators. Higher-order integrators are generally capable of dealing with this instability, but require many more score function evaluations.

To address this, we note that in isolation the kernel term has the form of a negative exponential centered on y, or explicitly:

$$z_{t+\Delta t} = y + (z_t - y)e^{\frac{\Delta t}{\lambda^2}}, \tag{14}$$

where Δt is negative. We take advantage of this to formulate a stable approximation that avoids the stability issues with a minimal change to the integration process. Instead of feeding the full composite score function to the integrator, in each time step we first integrate only the score function with the existing integrator to get ${z'}_{t+\Delta t}$. Immediately after, we separately account for the kernel term by computing the final output as

$$z_{t+\Delta t} = y + ({z'}_{t+\Delta t} - y)e^{\frac{\Delta t}{\lambda^2}}. \tag{15}$$

We note such numerically instability has been observed when using high CFG values. A remedy is to apply guidance in a limited interval (Kynkäänniemi et al., 2024). We leverage similar ad-hoc tricks by applying the kernel term in limited interval through the sampling chain.

4. Practical Implementation and Evaluation

In this section, we construct synthetic examples on which we demonstrate that our proposed method behaves as theory

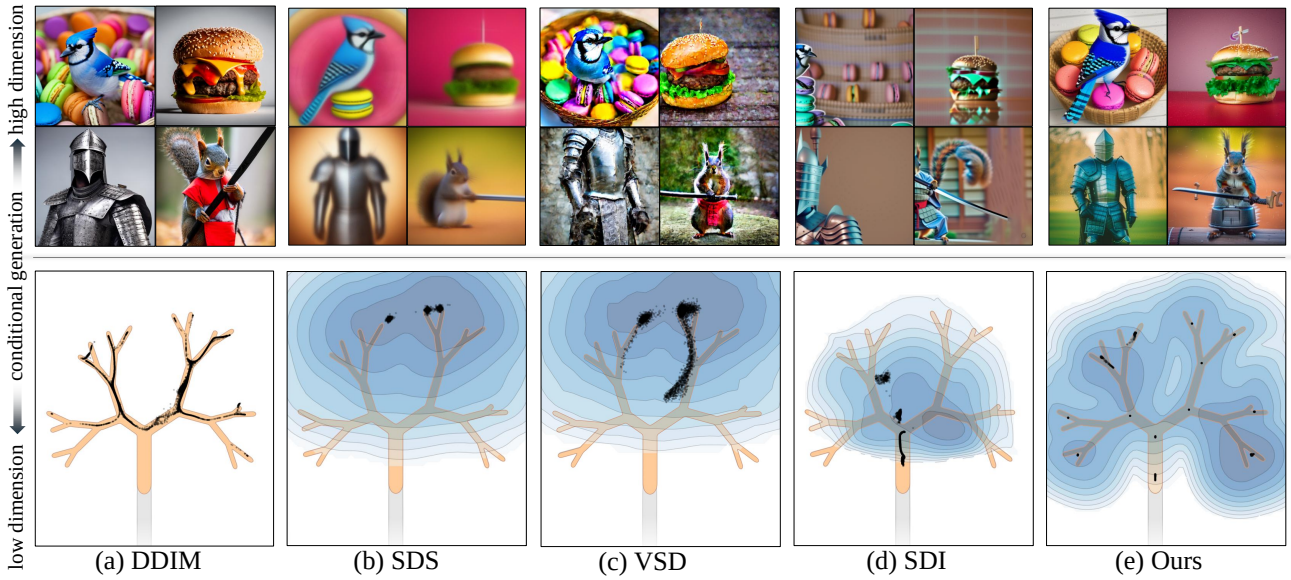

(a) DDIM (b) SDS (c) VSD (d) SDI (e) Ours

Figure 2: We juxtapose diffusion sampling vs diffusion distillation in low-dimensional ($\mathbb{R}^2$) and high-dimensional ($\mathbb{R}^{64\times64\times4}$) setting, using guidance via CFG (Ho & Salimans, 2021). **Top**: **(a)** text-conditioned generation of image via DDIM with 32 steps, **(b) - (e)** optimized coordinate-based neural implicit image for SDS, VSD, SDI, and our MSD respectively with StableDiffusion (CFG=7.5, § 4.4). **Bottom**: **(a)** class-conditioned generation of 2D points via DDIM with 32 steps, **(b) - (e)** optimized 2D points for SDS, VSD, SDI, and our MSD respectively (CFG=4, § 4.2). Text-prompts in clockwise order: *"A DSLR photo of a ... hamburger*, *squirrel dressed as a samurai weighing a katana*, *knight in silver armor*, and *bluejay on basket of macarons"*.

predicts, alleviating the issues SDS exhibits even in these simple scenarios. We further explain the issues encountered when translating this theory into practice, and describe adaptations we designed to make our method work with real-world diffusion models, retaining desirable properties. We make comparisons with two strong baselines that improve the convergence and performance of SDS; SDI (Lukoianov et al., 2024), who propose a better noise term to reduce late-stage stochasticity, yet, retain the same gradient computation of SDS, and VSD (Wang et al., 2023b), who propose to learn the variational score as opposed to assuming it to be a known analytic score like in SDS.

4.1. Idealized Setting

In order to manage large data dimensionality as well as massive training datasets, diffusion in practice employs a trained neural network to represent the denoiser D. However, (Karras et al., 2022; Je et al., 2024) have identified an analytical solution to minimizing the denoiser error, the *ideal denoiser* $D^*(x;t)$:

$$D^*(x;t) = \frac{\sum_i u_i \mathcal{N}(x;u_i,\sigma(t))}{\sum_i \mathcal{N}(x;u_i,\sigma(t))}, \tag{16}$$

where $u_0 \dots u_n$ are samples in our training set. Attentive readers will notice that this is in fact the discrete mean shift formula (Comaniciu & Meer, 2002), with training samples taking the place of data samples and noise magnitude $\sigma(t)$ taking place of the kernel bandwidth λ. This expression is feasible to compute in practice for small datasets, and by setting

$$\epsilon^*_\phi(z_t;t) = -\frac{D^*(z_t;t) - z_t}{\sigma_t},$$

we may substitute it into the SDS formula (1) to get an explicit solution for the SDS gradient

$$\nabla_x \mathcal{L}_{\text{SDS}} = \mathbb{E}_{t,z_t\sim\mathcal{N}(\alpha_t x,\sigma_t^2\mathbf{I})}\left[w(t)\frac{z_t - D^*(z_t;\sigma_t)}{\sigma_t}\frac{\partial x}{\partial\theta}\right].$$

We can brute force numerically evaluate this integral. We can compare both methods on synthetic datasets, eliminating any error introduced by training and evaluating a neural model to show that the theoretical properties hold.

4.2. Toy Distributions in $\mathbb{R}^2$

In addition to the fractal dataset (Figure 1), we extend our analysis to other 2D datasets, with $u_{i\,i=1}^{m} \subset \mathcal{M} \in \mathbb{R}^2$ sampled from various challenging toy 2D densities (van der Walt et al., 2014; Rozen et al., 2021). For each, we sample 10^4 points from the data distribution and initialize our target points densely across a grid $[-1.5, 1.5]^2$. With 10^3 Monte Carlo samples, we benchmark SDS, VSD, SDI, and our MSD (Algorithm 2) using both an ideal denoiser (16) and a

Table 1: Metrics for class-conditional distillation on 2D Fractal dataset. For each metric, *left* to *right*: ideal denoiser (D^*), learned denoiser (D_θ) without guidance, learned denoiser with CFG (Ho & Salimans, 2021), and learned denoiser with Autoguidance (Karras et al., 2024). 1st and 2nd best among distillation-based methods for each column, highlighted.

Method	NLL ↓			
DDIM	-1.85	-1.51	-1.59	-1.67
SDS	36.15	9.12	15.96	11.33
VSD	9.97	9.88	18.97	11.52
SDI	24.28	-2.87	27.37	0.65
Ours	-1.32	-2.02	-1.15	-1.99

Method	MMD ↓ (scaled by 10^{-4})			
DDIM	0.860	0.007	257.43	0.25
SDS	328.0	87.04	3875.11	71.05
VSD	230.9	94.68	3845.41	70.25
SDI	29.93	459.9	69.23	15089
Ours	30.46	12.79	133.41	122.94

Method	Precision ↑			
DDIM	0.97	0.95	0.97	0.96
SDS	0.08	0.01	0.17	0.04
VSD	0.05	0.10	0.21	0.03
SDI	0.27	0.97	0.30	0.51
Ours	0.92	0.97	0.94	0.97

Method	Recall ↑			
DDIM	0.93	0.96	0.44	0.79
SDS	0.03	0.00	0.03	0.03
VSD	0.02	0.05	0.05	0.03
SDI	0.01	0.12	0.48	0.51
Ours	0.33	0.42	0.40	0.43

Table 2: Metrics for unconditional distillation on 2D toy datasets. For each metric, *left* to *right*: ideal denoiser (D^*) and learned denoiser (D_θ). MMD scaled by 10^{-4}.

Dataset	Method	NLL ↓		Precision ↑		Recall ↑		MMD ↓	
Spiral	DDIM	-1.39	-1.32	0.97	0.96	0.93	0.96	0.410	1.160
	SDS	30.37	8.13	0.02	0.04	0.03	0.11	13.85	274.3
	VSD	10.15	8.90	0.04	0.07	0.09	0.14	23.46	271.8
	SDI	35.64	19.16	0.10	0.12	0.90	0.42	39.51	2008
	Ours	-1.28	-1.51	0.99	0.98	0.18	0.18	4.490	18.41
Pinwheel	DDIM	-1.19	-1.1	0.97	0.97	0.94	0.97	1.05	0.270
	SDS	2.29	2.00	0.85	0.90	0.03	0.01	5.18	36.37
	VSD	3.34	2.28	0.65	0.97	0.04	0.02	6.78	33.36
	SDI	28.31	17.33	0.17	0.51	0.001	0.15	6.13	98.09
	Ours	-1.94	-2.19	0.99	0.99	0.01	0.13	5.83	7.250

learned denoiser (13). For the fractal dataset the denoiser is class-conditioned; its score is either left unchanged (without guidance) or guided via CFG or Autoguidance. For the other datasets, the denoiser is unconditioned.

We visualize the generated samples produced by all methods after the optimization in Figures 2 and 3. We also visualize the reconstructed loss functions. This makes the behavior of all methods particularly obvious; the peaks of this reconstructed function are out of distribution for all methods except our MSD. Numerical evaluations in Tables 1 and 2 show our method outperform baselines. We suspect that this bias persists in SDS in higher dimensional settings and is what causes SDS optimized results to be blurry and exhibit other artifacts (top row of Figure 2).

For the learned denoiser, we use the architecture and training setup used by (Karras et al., 2024) and similarly represent the densities as mixtures of Gaussians. We use the Adam optimizer (Kingma & Ba, 2015) and run the optimization procedure for 150 steps with a learning rate of 0.08. For our MSD, we set an initial bandwidth of $0.316 \sim \sqrt{0.1}$ which is linearly decayed over the course of the optimization. For the ideal denoiser, due to it's high cost requirements in time and memory, we instead opt to use a few steps of gradient descent with high learning rate.

In addition to optimizing samples, we evaluate both SDS, VSD, SDI, and our MSD gradients across the domain and then numerically integrate them to reconstruct the loss functions they represent.

In addition to bias, we are interested in evaluating the variance of the gradient estimate. This is an important factor for convergence, since ascending a stochastic estimate of the gradient is essentially a random walk. In such, high variance of the estimate may make the walk take longer to converge – indeed, with sufficiently high variance we may

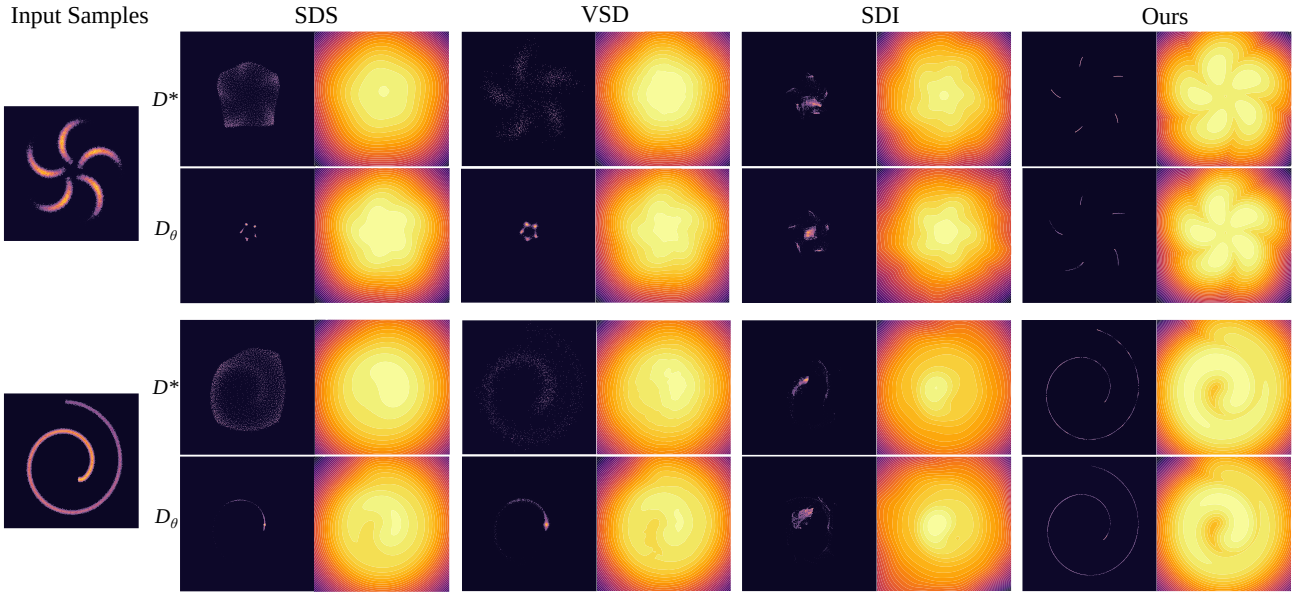

Figure 3: Unconditional distillation on two toy density datasets, *Pinwheel* (top) and *Spiral* (bottom), given an ideal denoiser (D^*) and a learned denoiser (D_θ). For each method and denoiser, we show the optimized samples (left) and the loss landscape (right). *Zoom in for clarity*.

find the iteration often taking *backwards* steps with respect to the true gradient. Furthermore, a walk with high variance may not stay converged at an optima, and instead randomly oscillate around them.

To quantify the variance of an estimate $\hat{g}(x)$ of the gradient $g(x)$, we employ a slight variation of the Monte Carlo estimator efficiency formula

$$\varepsilon(\hat{g}(x)) = \frac{|g(x)|^2}{\mathrm{MSE}(\hat{g}(x))\ \mathrm{cost}(\hat{g}(x))}. \tag{17}$$

We measure cost as number of invocations of the score model, since that is the typical bottleneck in diffusion.

Normalization by the squared norm of g is included to account for the fact that, due to bias and scaling, different estimators may converge to gradients of different magnitude, and the normalized MSE then roughly describes the probability of the estimated gradient pointing the "right" way. MSE and cost are accumulated over many independent estimations, and average over many values of x.

The result of these efficiency comparisons are in Table 3 (in log-scale). Although getting a single estimate with our method requires more score model invocations, the efficiency of our method is significantly higher than SDS and VSD, and comparable to SDI.

Table 3: Efficiency (↑) on 2D toy density datasets. *Left*: ideal denoiser / *Right*: learned denoiser.

	Fractal	**Spiral**	**Pinwheel**
SDS	-7.37 / -6.89	-8.48 / -7.57	-7.82 / -6.99
VSD	-5.92 / -3.83	-6.85 / -4.45	-6.36 / -3.93
SDI	14.18/ 14.21	13.94 / 14.17	14.19 / 14.18
Ours	13.44 / 7.65	13.38 / 6.32	13.76 / 7.08

4.3. Practical Setting

For large-scale image datasets, idealized denoiser is no longer tractable and we contend with a learned denoising function, and the associated machinery. This introduces numerical issues. Namely, the magnitude of the kernel term may grow to where the standard first or second order integrators can no longer manage it (Section 3.4); but conversely, so does the magnitude of the learned score when z_t is far out of distribution, because the ideal denoiser (Section 4.1) uses the same equation as mean shift. Start of the optimization, it is likely in a high-dimensional space that x will be out of distribution and we have to choose between the integration failing because the denoiser term has a high magnitude, or because the kernel term has a high magnitude.

To alleviate this, we use two heuristic approximations: applying guidance in limited interval (Section 3.4) and scaling our sample in Equation (15) by noise corresponding to time step t. In practice, we apply inversion to get the latter. These

Table 4: Text-to-2D quantitative comparison. We evaluate fidelity with FID and CLIP-SIM. †FID measured with DDIM as ground truth.

Method	FID ↓	CLIP-SIM (L/14) ↑
DDIM†	–	44.1± 2.8
SDS	198.90	27.7± 1.9
VDS	130.22	30.8± 1.4
SDI	166.16	31.0± 0.7
Ours	114.12	32.6± 0.8

are designed to keep the iterate in a region with reasonable score magnitude and still sample a distribution that is an approximation of the product distribution.

4.4. Pre-trained Stable Diffusion

We use the latent-space diffusion model, Stable Diffusion, as the diffusion prior for text-conditioned optimization of parameters of differentiable image generators. Specifically, we optimize parameters ϑ of generator g, a rendering function that maps ϑ to an image $\mathcal{I}$. The rendered image $\mathcal{I}$ is fed to the image encoder to get x^k, our latent at optimization step k, over which the gradient is computed. We define two settings where ϑ (1) represents an RGB image, and (2) represents a 3D volume. Specifically:

1. **Text-to-2D.** We represent 2D images via a coordinated-based MLP f with learnable parameters ϑ that takes as input a 2D point p in the unit square $p = (x, y) \in [0, 1]^2$ and outputs RGB $\in [0, 1]^3$; $f(p; \vartheta) : \mathbb{R}^2 \rightarrow$ RGB. We use this non pixel-based representation of an image for two reasons, (1) to prevent our method and the baselines from taking the exact gradient step i.e. running diffusion sampling and setting x^k to the denoised latent z_0, and (2) we can directly compare with images sampled via DDIM, an unconstrained image generation setting.

2. **Text-to-3D.** We represent 3D volumes as NeRFs, following (Poole et al., 2022). The NeRF is parameterized by two MLPs, one for foreground and one for background. The former has 64 hidden nodes and 2 layers, with input (x, y, z) coordinates encoded via HashGrid (Müller et al., 2022).

Implementation details. We implement all our code in PyTorch, on a single NVIDIA A100 gpu. We use the Threestudio (Guo et al., 2023) framework for experiments involving pre-trained Stable Diffusion. We use AdamW optimizer with lr$= 10^{-2}$. We set optimization steps to 400 for text-to-2D and $10k$ for text-to-3D. We use a monotonically decreasing schedule for the bandwidth λ.

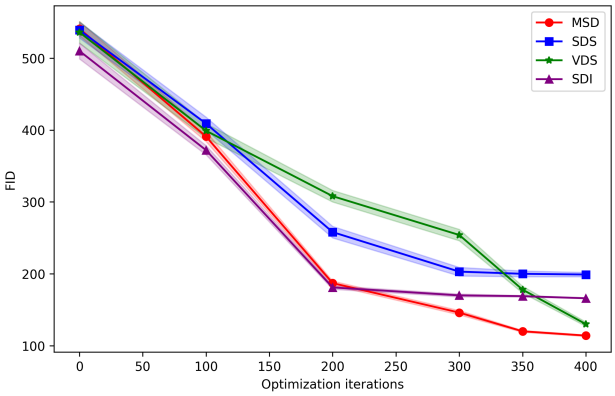

Figure 4: FID vs optimization iterations for text-to-2D generation.

Figure 5: Impact of bandwidth (λ) on the denoised latent (z_0). We set $\lambda_3 = 10^3$, $\lambda_2 = 10$, $\lambda_1 = 10^{-2}$. Highlighted images show the optimal bandwidth value corresponding to the k^{th} optimization.

4.5. Evaluation

Dataset. We use a subset of the prompts curated by (Poole et al., 2022; Hertz et al., 2023). We include all prompts in Appendix D.

Metrics. For toy density dataset (Section 4.2), we compute negative log-likelihood scores (NLL), generative precision and recall (Kynkäänniemi et al., 2019), and maximum mean discrepancy (MMD). For text-to-2D, we use images produced by DDIM to represent the ground truth distribution. To evaluate fidelity of the images, FID (Heusel et al., 2017) is computed for each baseline (SDS, VSD, SDI) and ours against this ground truth image set. We also compute CLIP scores (cli) to measure prompt-generation alignment.

Quantitative comparisons. Table 4 reports results for FID and CLIP-based similarity, comparing our method with SDS, VSD, and SDI. We outperform all baselines in image fidelity and achieve faster convergence, as measure via *fid* vs *iterations* in Figure 4.

Qualitative comparisons. Figure 2 (top row) and Figure 8 compares our method with SDS, VSD, and SDI on text-to-2D generation, qualitatively. We show the importance of the two heuristics (Section 4.3) to resolve numerical instabilities, absence of which can result in visual artifacts in Figure 9. SDS, as discussed, produces low-fidelity results while SDI's inversion accumulates numerical errors during early stages of optimization. In Figure 6, we qualitatively compare results for text-to-3D optimization. We restrict to qualitative comparison for this task as quantitative metrics have high variance due to the absence of a ground truth

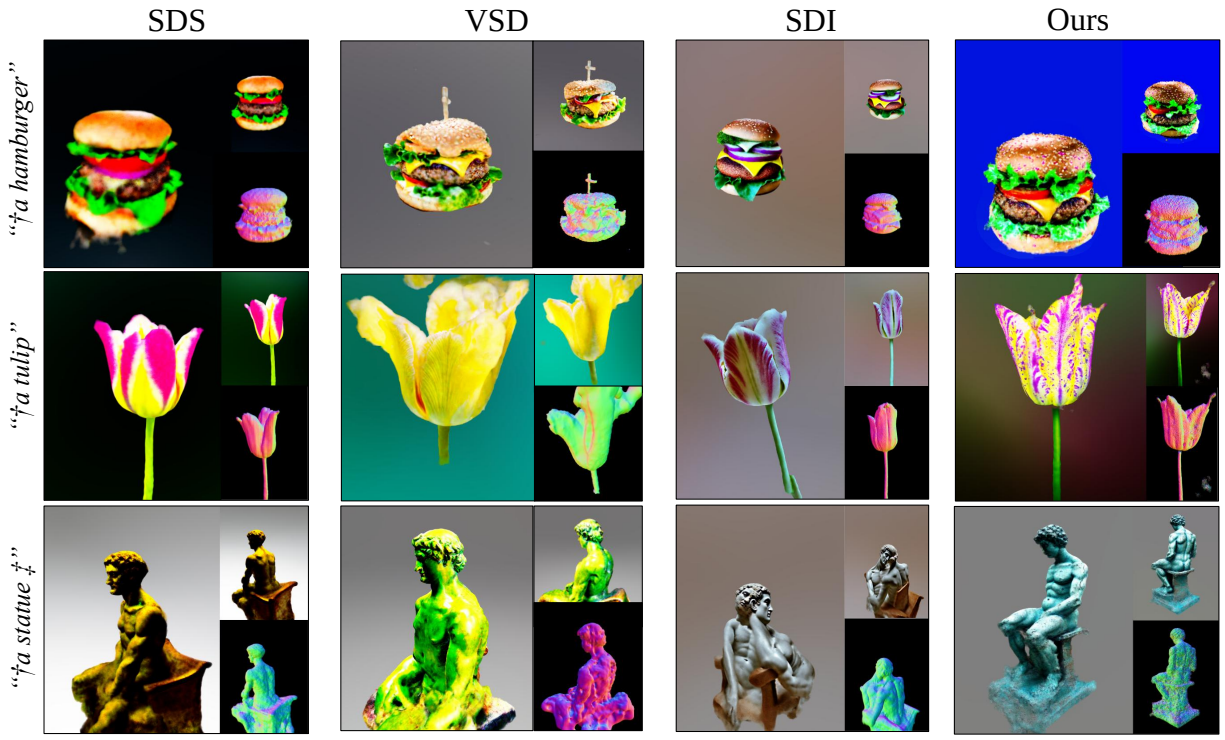

Figure 6: Comparison of 3D generation with other score distillation methods. Full prompt: † *"A DSLR photo of a ..."*, ‡ *"a Michelangelo statue of a man on a chair"*.

dataset.

Impact of bandwidth. Figure 5 shows the impact of the bandwidth (λ) term on the denoising process. First, we sample three parameters $\{\vartheta^k\}$ from our text-to-2D optimization pipeline at iterations $k = \{100, 200, 400\}$ and also sample three discrete λ values $\{\lambda_1 \ll \lambda_2 \ll \lambda_3\}$. Then, we run our forward pass once for each λ_i, independently. We visualize four decoded denoised latents z_0 (with different random seeds). The highlighted images show the optimal choices of λ for each x^k (the encoded latent for ϑ^k). At high bandwidth value λ_3, the influence of the kernel term in the product sampling is negligible. This degenerates to vanilla denoising and we observe high variance in the output, irrespective of our current x^k. This is ideal at early stages of optimization. As bandwidth is annealed, we observe reduction in variance. Yet, the quality of the outputs can degrade if the kernel term dominates while x^k is not *"in-distribution"*. As x^k approaches the mode of the distribution corresponding to the input text-prompt at final stages of optimization (when $k = 400$), with a low bandwidth λ_1, our denoised latent $z_0 \approx x^k$. This provides us with a convergence criteria and we terminate when λ is below the threshold λ_1.

5. Conclusion

In this paper, we have reframed diffusion distillation in terms of explicitly ascending the gradient of the data distribution. We have derived mean-shift distillation as a proxy that provably aligns with this gradient, and in the limit its maxima are collocated with the modes of the data distribution.

We have demonstrated that compared to SDS, this method achieves better mode alignment as well as lower gradient variance, which in practice translates to more realistic optimization results as well as improved convergence rate. Since this method simply provides optimization gradient much like SDS does, it may be used as a one-to-one replacement without retraining of the underlying model, or indeed substantial code modification.

While the basic algorithm works as the theory predicts in synthetic scenarios, with real-world models we have to contend with integrator error due to large score magnitudes. We have designed heuristics to alleviate this and achieve improvements on SDS in practice, but we hope future work will be able to improve the integration and/or sampling procedure, obviating the need for heuristics, in-addition to using adaptive bandwidth annealing strategies.

As a more or less straightforward substitute of an existing method (SDS), our method inherits ethical concerns of the diffusion models it is being applied to, and the applications it is being put towards. It remains important to take care with sourcing training data to avoid copyright issues, bias issues, and training harmful content into the model. On

the output side, generative models improve accessibility to creative expression, which however also makes it easier to produce harmful content including, but not limited to, misinformation, defamatory and obscene images. Ultimately these issues are impossible to fully solve on the tooling side and we must rely on other methods to analyse content and establish authenticity thereof to compensate.

That said, improved convergence properties of our method mean that less computation is required to achieve the same result, alleviating some of the environmental impacts associated with these generative methods.

Acknowledgments

The authors would like to thank Pradyumn Goyal, Dmitry Petrov, Ashish Singh, and Artem Lukoianov for their helpful discussions and insights. This project has received funding from the European Research Council (ERC) under the Horizon research and innovation programme (Grant agreement No. 101124742).

References

openai/clip-vit-large-patch14. https://torchmetrics.readthedocs.io/en/stable/multimodal/clip_score.html#id3.

Alldieck, T., Kolotouros, N., and Sminchisescu, C. Score distillation sampling with learned manifold corrective, 2024. URL https://arxiv.org/abs/2401.05293.

Bahmani, S., Skorokhodov, I., Rong, V., Wetzstein, G., Guibas, L., Wonka, P., Tulyakov, S., Park, J. J., Tagliasacchi, A., and Lindell, D. B. 4d-fy: Text-to-4d generation using hybrid score distillation sampling. *IEEE Conference on Computer Vision and Pattern Recognition (CVPR)*, 2024.

Belkin, M. and Niyogi, P. Laplacian eigenmaps for dimensionality reduction and data representation. *Neural Computation*, 15(6):1373–1396, 2003. doi: 10.1162/089976603321780317.

Bradley, A. and Nakkiran, P. Classifier-free guidance is a predictor-corrector, 2024. URL https://arxiv.org/abs/2408.09000.

Chen, D., Zhou, Z., Mei, J.-P., Shen, C., Chen, C., and Wang, C. A geometric perspective on diffusion models, 2024. URL https://openreview.net/forum?id=WTJv0L5QLX.

Cheng, Y. Mean shift, mode seeking, and clustering. *IEEE Transactions on Pattern Analysis and Machine Intelligence*, 1995. doi: 10.1109/34.400568.

Comaniciu, D. and Meer, P. Mean shift: A robust approach toward feature space analysis. *IEEE Trans. Pattern Anal. Mach. Intell.*, 24(5):603–619, 2002. URL http://dblp.uni-trier.de/db/journals/pami/pami24.html#ComaniciuM02.

Dhariwal, P. and Nichol, A. Diffusion models beat gans on image synthesis, 2021.

Grathwohl, W., Chen, R. T. Q., Bettencourt, J., and Duvenaud, D. Scalable reversible generative models with free-form continuous dynamics. In *International Conference on Learning Representations*, 2019. URL https://openreview.net/forum?id=rJxgknCcK7.

Guo, Y.-C., Liu, Y.-T., Shao, R., Laforte, C., Voleti, V., Luo, G., Chen, C.-H., Zou, Z.-X., Wang, C., Cao, Y.-P., and Zhang, S.-H. threestudio: A unified framework for 3d content generation. https://github.com/threestudio-project/threestudio, 2023.

Hertz, A., Aberman, K., and Cohen-Or, D. Delta denoising score. 2023.

Heusel, M., Ramsauer, H., Unterthiner, T., Nessler, B., and Hochreiter, S. Gans trained by a two time-scale update rule converge to a local nash equilibrium. In *Proceedings of the 31st International Conference on Neural Information Processing Systems*, NIPS'17, pp. 6629–6640, Red Hook, NY, USA, 2017. Curran Associates Inc. ISBN 9781510860964.

Ho, J. and Salimans, T. Classifier-free diffusion guidance. In *NeurIPS 2021 Workshop on Deep Generative Models and Downstream Applications*, 2021. URL https://openreview.net/forum?id=qw8AKxfYbI.

Jain, A., Xie, A., and Abbeel, P. Vectorfusion: Text-to-svg by abstracting pixel-based diffusion models. In *Proceedings of the IEEE/CVF Conference on Computer Vision and Pattern Recognition*, pp. 1911–1920, 2023.

Je, J., Liu, J., Yang, G., Deng, B., Cai, S., Wetzstein, G., Litany, O., and Guibas, L. Robust symmetry detection via riemannian langevin dynamics. In *SIGGRAPH Asia 2024 Conference Papers*, SA '24, New York, NY, USA, 2024. Association for Computing Machinery. ISBN 9798400711312. doi: 10.1145/3680528.3687682. URL https://doi.org/10.1145/3680528.3687682.

Karras, T., Aittala, M., Aila, T., and Laine, S. Elucidating the design space of diffusion-based generative models. In *Proc. NeurIPS*, 2022.

Karras, T., Aittala, M., Kynkäänniemi, T., Lehtinen, J., Aila, T., and Laine, S. Guiding a diffusion model with a bad version of itself. In *The Thirty-eighth Annual*

Conference on Neural Information Processing Systems, 2024. URL https://openreview.net/forum?id=bg6fVPVs3s.

Katzir, O., Patashnik, O., Cohen-Or, D., and Lischinski, D. Noise-free score distillation. In *The Twelfth International Conference on Learning Representations*, 2024. URL https://openreview.net/forum?id=dlIMcmlAdk.

Kingma, D. P. and Ba, J. Adam: A method for stochastic optimization. In Bengio, Y. and LeCun, Y. (eds.), *3rd International Conference on Learning Representations, ICLR 2015, San Diego, CA, USA, May 7-9, 2015, Conference Track Proceedings*, 2015. URL http://arxiv.org/abs/1412.6980.

Kynkäänniemi, T., Aittala, M., Karras, T., Laine, S., Aila, T., and Lehtinen, J. Applying guidance in a limited interval improves sample and distribution quality in diffusion models. In *The Thirty-eighth Annual Conference on Neural Information Processing Systems*, 2024. URL https://openreview.net/forum?id=nAIhvNy15T.

Kynkäänniemi, T., Karras, T., Laine, S., Lehtinen, J., and Aila, T. Improved precision and recall metric for assessing generative models. *CoRR*, abs/1904.06991, 2019.

Liang, Y., Yang, X., Lin, J., Li, H., Xu, X., and Chen, Y. Luciddreamer: Towards high-fidelity text-to-3d generation via interval score matching. *arXiv preprint arXiv:2311.11284*, 2023.

Lukoianov, A., de Ocáriz Borde, H. S., Greenewald, K., Guizilini, V. C., Bagautdinov, T., Sitzmann, V., and Solomon, J. Score distillation via reparametrized ddim, 2024.

Luo, W., Hu, T., Zhang, S., Sun, J., Li, Z., and Zhang, Z. Diff-instruct: A universal approach for transferring knowledge from pre-trained diffusion models. In *Thirty-seventh Conference on Neural Information Processing Systems*, 2023. URL https://openreview.net/forum?id=MLIs5iRq4w.

Müller, T., Evans, A., Schied, C., and Keller, A. Instant neural graphics primitives with a multiresolution hash encoding. *ACM Trans. Graph.*, 41(4):102:1–102:15, July 2022. doi: 10.1145/3528223.3530127. URL https://doi.org/10.1145/3528223.3530127.

Poole, B., Jain, A., Barron, J. T., and Mildenhall, B. Dreamfusion: Text-to-3d using 2d diffusion. *arXiv*, 2022.

Roweis, S. T. and Saul, L. K. Nonlinear Dimensionality Reduction by Locally Linear Embedding. *Science*, 2000. doi: 10.1126/science.290.5500.2323. URL http://www.sciencemag.org/cgi/content/abstract/290/5500/2323.

Rozen, N., Grover, A., Nickel, M., and Lipman, Y. Moser flow: Divergence-based generative modeling on manifolds, 2021. URL https://arxiv.org/abs/2108.08052.

Song, J., Meng, C., and Ermon, S. Denoising diffusion implicit models. In *International Conference on Learning Representations*, 2021a. URL https://openreview.net/forum?id=St1giarCHLP.

Song, Y., Sohl-Dickstein, J., Kingma, D. P., Kumar, A., Ermon, S., and Poole, B. Score-based generative modeling through stochastic differential equations. In *International Conference on Learning Representations*, 2021b. URL https://openreview.net/forum?id=PxTIG12RRHS.

Thamizharasan, V., Liu, D., Fisher, M., Zhao, N., Kalogerakis, E., and Lukac, M. Nivel: Neural implicit vector layers for text-to-vector generation. In *Proceedings of the IEEE/CVF Conference on Computer Vision and Pattern Recognition (CVPR)*, pp. 4589–4597, June 2024.

Thamizharasan, V., Chatzis, N., Georgiev, I., Fisher, M., Kalogerakis, E., Liu, D., Zhao, N., and Lukac, M. Mean-shift distillation for diffusion mode seeking, 2025. URL https://arxiv.org/abs/2502.15989.

van der Walt, S., Schönberger, J. L., Nunez-Iglesias, J., Boulogne, F., Warner, J. D., Yager, N., Gouillart, E., Yu, T., and the scikit-image contributors. scikit-image: image processing in Python. *PeerJ*, 2:e453, 6 2014. ISSN 2167-8359. doi: 10.7717/peerj.453. URL https://doi.org/10.7717/peerj.453.

Wang, H., Du, X., Li, J., Yeh, R. A., and Shakhnarovich, G. Score jacobian chaining: Lifting pretrained 2d diffusion models for 3d generation. *arXiv preprint arXiv:2212.00774*, 2022.

Wang, P., Fan, Z., Xu, D., Wang, D., Mohan, S., Iandola, F., Ranjan, R., Li, Y., Liu, Q., Wang, Z., et al. Steindreamer: Variance reduction for text-to-3d score distillation via stein identity. *arXiv preprint arXiv:2401.00604*, 2023a.

Wang, P., Xu, D., Fan, Z., Wang, D., Mohan, S., Iandola, F., Ranjan, R., Li, Y., Liu, Q., Wang, Z., and Chandra, V. Taming mode collapse in score distillation for text-to-3d generation. *arXiv preprint: 2401.00909*, 2024.

Wang, Z., Lu, C., Wang, Y., Bao, F., Li, C., Su, H., and Zhu, J. Prolificdreamer: High-fidelity and diverse text-to-3d generation with variational score distillation. In *Advances in Neural Information Processing Systems (NeurIPS)*, 2023b.

Xie, S., Xiao, Z., Kingma, D. P., Hou, T., Wu, Y. N., Murphy, K. P., Salimans, T., Poole, B., and Gao, R. EM distillation for one-step diffusion models. In *The Thirty-eighth Annual Conference on Neural Information Processing Systems*, 2024. URL https://openreview.net/forum?id=rafVvthuxD.

Xu, Y., Srinivasa, J., Liu, G., and Tulsiani, S. Diverse score distillation, 2024. URL https://arxiv.org/abs/2412.06780.

Yan, R., Chen, Y., and Wang, X. Consistent flow distillation for text-to-3d generation, 2025. URL https://arxiv.org/abs/2501.05445.

Yi, T., Fang, J., Wang, J., Wu, G., Xie, L., Zhang, X., Liu, W., Tian, Q., and Wang, X. Gaussiandreamer: Fast generation from text to 3d gaussians by bridging 2d and 3d diffusion models. In *CVPR*, 2024.

Yin, T., Gharbi, M., Zhang, R., Shechtman, E., Durand, F., Freeman, W. T., and Park, T. One-step diffusion with distribution matching distillation. In *CVPR*, 2024.

Yu, X., Guo, Y.-C., Li, Y., Liang, D., Zhang, S.-H., and QI, X. Text-to-3d with classifier score distillation. In *The Twelfth International Conference on Learning Representations*, 2024. URL https://openreview.net/forum?id=ktG8Tun1Cy.

A. Implementation details

Input : pre-trained diffusion model $\epsilon_\theta : \mathbb{R}^{d_1 \times \cdots \times d_k} \to \mathbb{R}^{d_1 \times \cdots \times d_k}$, target parameters $\psi \in \mathbb{R}^d$, condition c, mapping function $g(\psi) : \mathbb{R}^d \to \mathbb{R}^{d_1 \times \cdots \times d_k}$, time-dependent functions $w(t), \alpha(t)$, Monte Carlo sample size N.
Output : ψ^*

Algorithm 1: Distillation via SDS

for $k = 1, \ldots, steps$ **do**
  $x^k \leftarrow g(\psi)$
  for $i = 1, \ldots, N$ **do**
    $t \leftarrow \mathrm{U}(0, 1)$
    $z_t \leftarrow \alpha(t)x^k + \epsilon_t$
    $y_i \leftarrow w(t)[\epsilon_\theta(z_t, t, c) - \epsilon_t]$
  $\nabla_\psi \mathcal{L}_{SDS} \leftarrow \frac{1}{N}\sum(y_i - x^k)$
  // Backpropagate $\nabla_\psi \mathcal{L}_{SDS}$, update ψ

Algorithm 2: Distillation via MSD (Ours)

function *ODESolver*(x, λ) *(eq 12)*
  $z_T \leftarrow \mathcal{N}(0, I)$
  for $t = T, \ldots, 1$ **do**
    $z_{t-1} \leftarrow \epsilon_\theta(z_t, t, c) - (x - z_t)/\lambda^2$
  return z_0
function *ODESolver*$(x, \lambda,$ *stable) (eq 15)*
  $\{z_t^*\}_{t=1}^T \leftarrow inversion(x)$
  $z_T \leftarrow z_T^* + (\epsilon - z_T^*)e^{-\Delta t/\lambda^2}$
  for $t = T, \ldots, 1$ **do**
    $z_{t-1} \leftarrow z_t^* + (\epsilon_\theta(z_t, t, c) - z_t^*)e^{-\Delta t/\lambda^2}$
  return z_0
// initialize λ, set λ_{min}
for $k = 1, \ldots, steps$ **do**
  $x^k \leftarrow g(\psi)$
  for $i = 1, \ldots, N$ **do**
    $y_i \leftarrow \mathrm{ODESolver}(x^k, \lambda)$
  $\nabla_\psi \mathcal{L}_{MSD} \leftarrow \frac{1}{N}\sum_i^N (y_i - x^k)$
  // Backpropagate $\nabla_\psi \mathcal{L}_{MSD}$, update ψ
  // Anneal λ
  if $\lambda < \lambda_{min}$ **then**
    // terminate

Figure 7: Pseudocode of SDS and our procedure, MSD. We additionally show the numerically stable solver, *ODESolver(. . . , stable)*, which is used for experiments with Stable Diffusion. Note, there is stochasticity in the *ODESolver*.

B. Discussions

Why mode-seeking? The desirability of mode seeking varies between applications. When trying to directly sample images from the trained model, we wish to sample from the full variety of the distribution instead of getting only the mode— we want sampling to interpolate between mode-seeking and mode-covering. Methods like DDIM aim for this. On the other hand, when we are optimizing an image (or using the image as a proxy to optimize, e.g. NeRF parameters), any gradient-based optimization will converge to a set of sparse points - local extrema - where the gradients are zero (if it converges at all). This is the intended use-case for SDS, VSD, SDI, and our method, and in this case, it is not possible in general to have the optimization process converge to a distribution of points. Given that, the best we can guarantee is that the points the process converges to are aligned with the distribution. Mode-seeking is our proposed way of achieving that.

Compatibility with other guidance schemes. In low-dimensional settings (eg, our toy experiments), our method can recover the modes and reconstruct the data distribution well without any guidance (See Figures 1 and 3). This is aided by the fact that the conditional score estimates parameterized as $\epsilon_\theta(z_t, c)$ (predicted noise from the pre-trained network) is good by itself, without guidance i.e. $\tilde{\epsilon}_\theta(z_t, c)$. Empirically, we observe that without guidance, ancestral sampling techniques like DDIM produce samples that lie on the data manifold, albeit with few outliers.

This is not the case in the high-dimensional setting with experiments on Stable Diffusion. Here $\epsilon_\theta(z_t, c)$ samples are noticeably bad and are predominantly outliers. Currently, the best fix is to augment these noise estimates with guidance to produce $\tilde{\epsilon}_\theta(z_t, c)$, the strategy prevalent in sampling algorithms. We inherit these practices when performing distillation.

Guidance mechanisms alternative to CFG (Ho & Salimans, 2021) have been proposed, like Autoguidance (Karras et al., 2024). As these methods pair well with DDIM (and other ancestral sampling techniques), we believe the benefits will extend

to distillation-based methods like ours. Ultimately from the perspective of distillation, different guidance simply changes the shape of the output distribution but does not fundamentally change the mechanics of diffusion. While we show results using Autoguidance in Table 1, we used CFG in all the remaining experiments as it is more widely used, has hyperparameters (guidance scale) that have been more rigorously tested by the community, and was used in all our baselines (SDS, VSD, and SDI).

C. Ablations and More Results

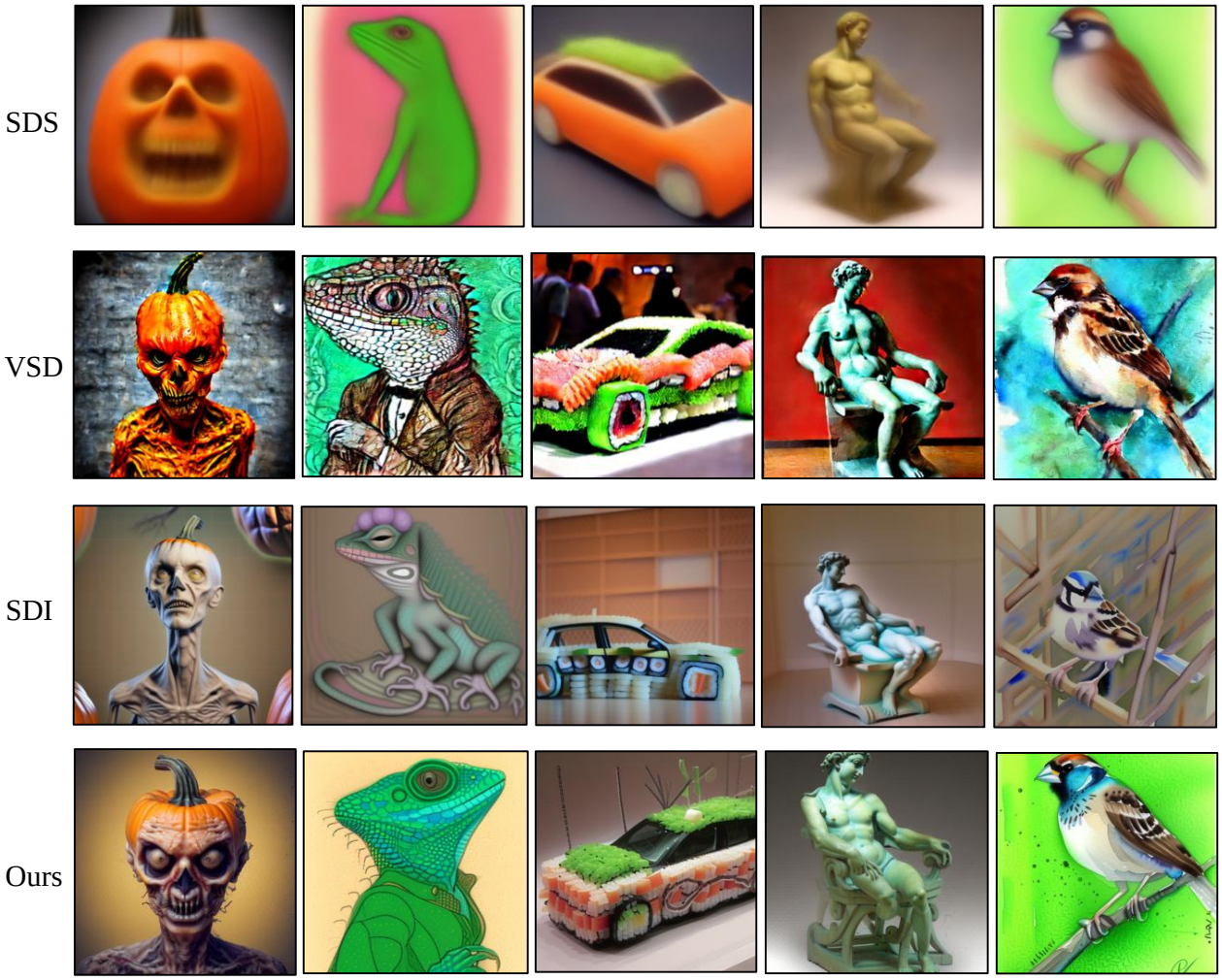

Figure 8: We also show additional results for our method (full), SDI, VSD, and SDS.

D. List of prompts

"A DSLR photo of a hamburger"

"A blue jay standing on a large basket of rainbow macarons"

"A DSLR photo of a squirrel dressed as a samurai weighing a katana"

"A DSLR photo of a knight in silver armor"

"Line drawing of a Lizard dressed up like a victorian woman, lineal color"

"A photo of a car made out of sushi"

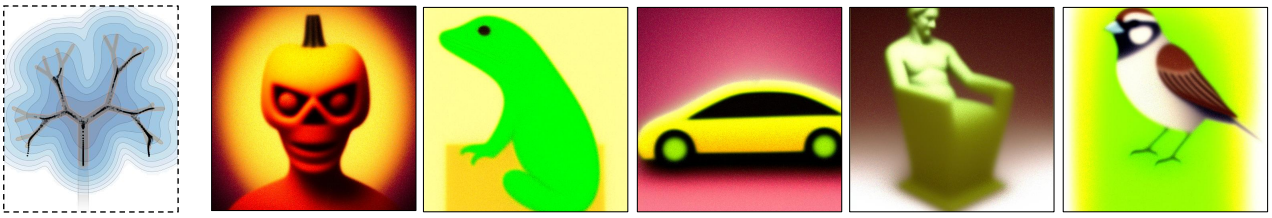

Ours (without guidance in limited interval and noise scaling/ inversion)

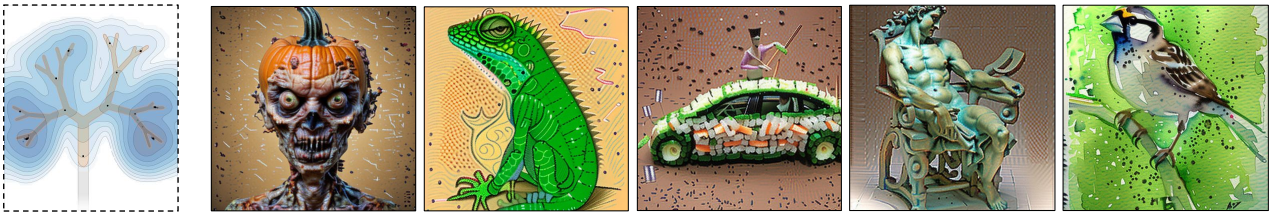

Ours (without guidance in limited interval)

Figure 9: We extend Figure 2 with two ablations; applying guidance in the entire denoising trajectory (row 1) and noise scaled sample in the kernel term (row 2) (§ 4.3).

"A DSLR photo of a tulip"

"A DSLR photo of a Pumpkin head zombie, skinny, highly detailed, photorealistic"

"A watercolor painting of a sparrow, trending on artstation"

"Michelangelo style statue of man sitting on a chair"

E. Licenses

Here we provide the URL, citations and licenses of the open-sourced assets we use in this work.

Table 5: URL, citations and licenses of the open-sourced assets we use in this work.

URL	Citation	License
https://github.com/threestudio-project/threestudio	[39]	Apache License 2.0
https://github.com/Stability-AI/stablediffusion	[39]	MIT License
https://github.com/NVlabs/edm2	[12]	CC BY-NC-SA 4.0